MICRO-SCALE LASER SHOCK PROCESSING – MODELING, TESTING, AND MICROSTRUCTURE CHARACTERIZATION

Wenwu Zhang and Y. Lawrence Yao
Department of Mechanical Engineering
Columbia University
New York, NY 10027

ABSTRACT

This paper reports modeling improvements for micro-scale laser shock processing (LSP), fatigue testing of shock processed copper samples, and microstructure characterization of shock processed materials (Cu and Ni). Plasma expansion is modeled as laser supported combustion wave, in which radial and axial expansions are considered. Stress/strain analysis is extended to three-dimensional and takes into account of finite geometry, which is important for micro-scale LSP. Tests are designed to demonstrate that micro-scale LSP can improve fatigue performance of the materials while offering a level of flexibility. The influence of LSP on the microstructures of the materials is studied quantitatively using Orientation Imaging Microscope (OIM) technique, and grain size and subgrain structures are analyzed.

1 INTRODUCTION

The expanding applications of micro devices make the mechanical properties of such devices an increasing concern. Processes that can improve the mechanical properties at micro scale are required. Laser Shock Processing (LSP) at the millimeter scale (i.e., the focused laser beam diameter in the order of millimeters) has been used to improve the hardness, residual stress distributions, and thus fatigue life of metals (Clauer et al., 1981; Peyre et al., 1995; Berthe et al., 1998). More recently, laser shock processing of aluminum and copper at micro-scale has been studied (Zhang and Yao, 2000a & b). The reduced scale requires reconsideration of a number of issues.

Previous shock pressure models assumed that a constant fraction of plasma internal energy α was assumed to increase the pressure of the plasma (Clauer et al., 1981, Fabbro et al., 1990, and Zhang and Yao, 2000a & b). The way in which α was experimentally determined is rather cumbersome and indirect, and this value varied from 0.1 to 0.4 across different literature. The reason is that in previous models there was no consideration of mass exchanges between plasma and confining medium (e.g., water) or plasma and target, only energy and momentum conservation were considered. Explicit consideration of the mass transfer in the model will eliminate the need for prescribing the value of α and thus reduce the arbitrariness and increase the model accuracy, which is crucial for the micro scale under consideration.

Dynamic deformation process of the target material under the action of shock load had been simulated using the finite element method (FEM), but only for the 1D case (Clauer et al., 1981; Peyre et al., 1995; Berthe et al., 1998) and the axisymmetric case (Zhang and Yao, 2000a & b) where semi-infinity boundary conditions were

implicitly assumed. Effects of finite size and complex geometry on shocking results were neglected and in fact they are very important in practice, especially for LSP of small components and LSP near edges of the components.

Fatigue life of shock-processed samples can be improved due to shock induced compressive residual stresses (Clauer et al., 1981; Zhang and Yu, 1998). Comparable study of micro-scale LSP was not available. Experimental condition of micro-scale LSP is very different from mm-scale LSP. The fatigue mechanism of micro-scale LSP requires further investigation.

Mechanical properties of shocked materials are closely related to their microstructures including sub-grain structures. The microstructure change in LSP was primarily studied using transmission electron microscopy (TEM) in the past, where increases of twinning and dislocation structures were reported (Murr, 1981). Statistical and quantitative analysis of microstructure especially sub-grain structure change accompanying LSP is desired but is inherently difficult using TEM.

In this paper, the expansion of plasma is modeled as 1D laser supported combustion (LSC) wave. The 1D results are then modified to consider spatial expansion effects of the shock pressure. Copper and nickel samples are processed using micro-scale LSP and are compared with raw materials in terms of fatigue performance. 3D simulations of the shock induced deformation process are carried out, where the effects of finite sample size and irregular geometry are considered. The Orientation Imaging Microscope (OIM) techniques are used to quantitatively and statistically characterize the microstructures of laser shock processed samples.

2 MODELING OF LASER INDUCED SHOCK WAVES

When a short and intense laser pulse is irradiated onto a coated metallic target, the coating instantaneously vaporizes into a high temperature and high pressure plasma. This plasma induces shock waves during expansion from the irradiated surface, and mechanical impulses are transferred to the target. If it is confined by a liquid (e.g., water) or another type of medium, the shock pressure can be magnified by a factor of 5 or more compared with the open-air condition (Fox, 1974). Under typical conditions of LSP, the speed of plasma expansion is lower than the shock speed, thus shock wave precedes plasma expansion. This resembles the case of laser supported combustion (LSC) wave (Root, 1989). LSC wave in air and vacuum has been studied (Pirri et al., 1978) and will be extended in this paper to LSP modeling.

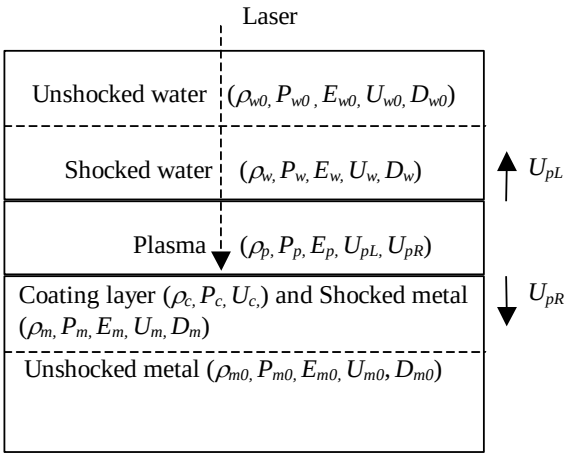

FIG. 1 FIVE REGIONS IN WATER CONFINED LSP.

In LSP, laser irradiation first vaporizes the surface layer of the coating, and the vaporized material quickly evolves into plasma. Water near the plasma outer edge is changed into plasma due to plasma irradiation and direct laser irradiation. Mass, momentum and energy are conserved across the shock wave. To model the process, the following assumptions are made.

(1) The early stage of plasma expansion is one-dimensional.
(2) Plasma obeys ideal gas laws.
(3) Only the coating layer is vaporized, the metal target experiences negligible thermal effects.
(4) The coating layer is thin and well coupled with the metal target, thus the shock pressure and the particle velocity of the coating layer and the metal target are equal.

Let subscripts *w* denote water, *m* metal, *c* the coating layer, *p* plasma, *L* the side of plasma near water, *R* the side of plasma near solid, and *0* the property of unshocked region. Also let *D* be shock velocity, *U* particle velocity, *E* internal energy, ρ density, and *P* pressure. For convenience, the water-plasma-target system is divided into five regions (Fig. 1): unshocked water (ρ_{w0}, P_{w0}, E_{w0}, U_{w0}, D_{w0}), shocked water (ρ_w, P_w, E_w, U_w, D_w), plasma (ρ_p, P_p, E_p, U_{pL}, U_{pR}),

coating layer and shocked solid (ρ_c, P_c, U_c, ρ_m, P_m, E_m, U_m, D_m), and unshocked solid(ρ_{m0}, P_{m0}, E_{m0}, U_{m0}, D_{m0}). The unshocked properties are known. The shocked and unshocked properties of water are related by mass, momentum, and energy conservation, and shock speed constitutive relations:

$$\rho_{w0}/\rho_w = 1-(U_w - U_{w0})/(D_w - U_{w0}) \quad (1)$$

$$P_w - P_{w0} = \rho_{w0}(D_w - U_{w0})(U_w - U_{w0}) \quad (2)$$

$$(E_w + U_w^2/2) - (E_{w0} + U_{w0}^2/2) = \frac{1}{2}(P_w + P_{w0})\left(\frac{1}{\rho_{w0}} - \frac{1}{\rho_w}\right) \quad (3)$$

$$D_w = D_{w0} + S_w U_w \quad (4)$$

For water, U_{w0} = 0 m/s, P_{w0} = 10^5 Pa, E_{w0} = 0 J/kg, ρ_{w0} = 997.9 kg/m^3, D_{w0} = 2,393 m/s, and S_w = 1.333 (Assay and Shahinpoor, 1992). S_w is a coefficient relating shock speed D_w to U_w, the particle velocity and D_{w0}, the shock speed at infinitesimally small particle velocity. Substituting subscript *m* for *w* in Eq. 1-4, one obtains four more equations between shocked and unshocked properties of metals. U_{m0} = 0 m/s, P_{m0} = 10^5 Pa, E_{m0} = 0 J/kg. For copper, ρ_{m0} = 8,939 kg/m^3, D_{m0} = 3,933 m/s, and S_m = 1.489. For nickel, ρ_{m0} = 8,874 kg/m^3, D_{m0} = 4,581 m/s, and S_m = 1.463 (Meyers and Murr, 1981).

The above equations can be solved after considering their interactions with the plasma. Mass and momentum conservation at the interfaces at any instant requires:

$$\rho_w(U_{pL} - U_w) = \rho_p U_{pL} \quad (5)$$

$$\rho_c(U_{pR} - U_c) = \rho_c Vrec = \rho_p U_{pR} \quad (6)$$

$$P_p + \rho_p U_{pR} U_c = P_c \quad (7)$$

$$P_p + \rho_p U_{pR} U_w = P_w \quad (8)$$

The current mass of the plasma is equal to the integration of the mass flows into plasma. The mass flow from water is $MF_w = \rho_w(U_{pL} - U_w)$. The mass flow from the coating layer is: $MF_c = \rho_c(U_{pR} - U_c) = \rho_c Vrec$, where *Vrec* is the recess velocity of the melting coat surface. According to assumption 4, $U_m = U_c$, and $P_m = P_c$. The mass conservation of plasma requires:

$$\rho_P(t)\int_0^t (U_{pL} + U_{pR})dt = \int_0^t (MF_w + MF_c)dt \quad (9)$$

The energy conservation of plasma should consider the absorption of incident laser irradiation, the total energy stored in the plasma E_{pt}, the work done by the plasma W_p, and energy exchanges through mass flow E_{MF}. Let *AP* be the fraction of laser energy absorbed by plasma, and *I(t)* the laser intensity, the energy conservation of plasma requires:

$$E_{pt} + W_p - E_{MF} = \int_0^t AP \times I(t)dt \quad (10)$$

Using the ideal gas law, the internal energy of plasma is related to its density, specific heat ratio γ (about 1.3), and pressure:

$$E_p = \frac{\gamma P_p}{(\gamma - 1)\rho_p} \quad (11)$$

This 1D LSP model can be solved as a function of time. Radial and axial expansion of plasma is a more significant concern in micro-scale LSP than in mm-scale LSP. Based on the work of Pirri (1978), Simons (1984), and Root (1989), the power scaling laws are used to describe the temporal evolution of shock pressure and plasma radius (Zhang and Yao, 2001).

For laser shock processing on micron scale, the spatial profile of the laser beam should also be considered. Following the work of Zhang and Yao (2000a), let *R(t)* be the radius of plasma, *r* be the radial distance from the center of the laser beam, then the spatially uniform shock pressure *P(t)* relates to the spatially non-uniform shock pressure as

$$P(r,t) = P(t)\exp\left(-\frac{r^2}{2R^2(t)}\right) \quad (12)$$

3 EXPERIMENTAL AND SIMULATION CONDITIONS

3.1 Experimental Conditions

Micro-scale LSP can be applied to a variety of metals. Copper and nickel are chosen in this study because they are often etched and deposited on silicon substrates as part of micro devices. Nickel is also used as a metallic MEMS material. The mechanical properties of nickel and copper are different. For instance, the Young's modulus of copper and nickel are 120 and 220 GPa, respectively. The ultimate strengths of annealed copper and nickel are 215 and 400 MPa, respectively.

Copper foils of 90-micron thickness and nickel foils of 120-micron thickness were used in LSP

experiments. The samples were adhesively attached to bulk copper columns for rigid support and easy handling. To apply the coating, a thin layer of high vacuum grease (about 10 microns) was spread evenly on the polished sample surface, and the coating material, aluminum foil of 25 microns thick is then tightly pressed onto the grease. The sample was placed in a shallow container filled with distilled water around 3 mm above the sample. A frequency tripled Q-switched Nd:YAG laser in TEM_{00} mode was used, the pulse duration was 50 ns. Laser beam diameter is 12 microns. After shock processing, the coating layer and the vacuum grease were manually removed. Pulse number at each location was varied from 1 to 6 at 1 kHz repetition rate, and pulse energy was varied from 160 μJ to 240 μJ corresponding to laser intensity of 2.83 to 4.24 GW/cm^2. LSP at individual locations (similar to drilling) and overlapped locations (similar to grooving) was carried out.

The geometry of the shocked region was measured using optical microscopy, scanning electron microscopy (SEM), and interferometry-based optical profilometry. Fatigue tests and Orientation Imaging Microscopy (OIM) measurements of microstructures were also carried out. Details of these measurements are described in the results and discussion part.

3.2 Simulation Conditions

The spatial and temporal dependent shock pressure was solved numerically based on what was outlined in Section 2 and used as the loading for the subsequent stress/strain analysis. In the stress/strain analysis, work hardening, strain rate and pressure effects on yield strength are considered (Zhang and Yao, 2000a) assuming room temperature. This is reasonable because only the coating is vaporized and minimal thermal effects are felt by the sample. A commercial FEM code, ABAQUS, is used for the stress/strain analysis as a dynamic implicit nonlinear process. First, axisymmetric modeling was carried out to compare the effects of the current shock pressure model with the previous model on deformation (Zhang and Yao, 2000a) assuming semi-infinity geometry. Secondly, 3D simulation was carried out assuming finite geometry. 3D simulations were extended to consider the specimen geometry used in the fatigue tests. The geometry and finite size effects were studied to explain the fatigue test results.

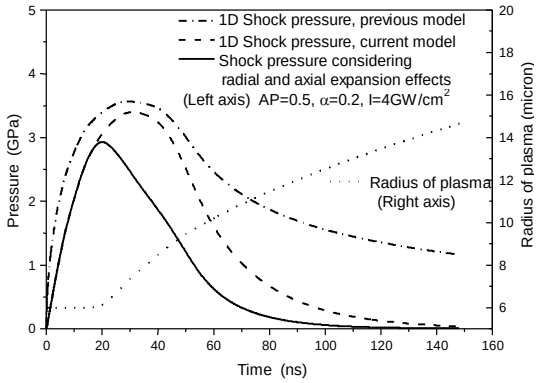

FIG. 2 SHOCK PRESSURE COMPARISON OF CURRENT MODEL AND PREVIOUS MODEL (ZHANG AND YAO, 2000A) AND CONSIDERATION OF SPATIAL EFFECTS.

4. RESULTS AND DISCUSSION

4.1 Results of Shock Pressure Modeling

In previous modeling work, mass flow from water into plasma and from target into plasma along with the property changes of water, target and plasma, are neglected (Fabbro et al., 1990; Zhang and Yao, 2000a). In fact, plasma grows as the target material and water breakdown into plasma. The evolution of mass flow from water into plasma can be studied using current LSP model (Zhang and Yao, 2001). Fig. 2 compares the 1D shock pressure determined using the current model and previous model (Zhang and Yao, 2000a) at laser intensity of 4 GW/cm^2. The previous model assumed that a constant fraction α = 0.2 of plasma energy is used to increase the shock pressure during the expansion of the plasma. In the current model such conversion is inherently considered in the energy balance relations. As seen, the previous model determined a higher peak pressure at laser intensity of 4 GW/cm^2. The pressure recovers to zero values faster in the current model than in the previous model. The reason is that in the current model, plasma energy is used for the breakdown of water and target material besides the expansion of plasma, while in the previous model only the 1D expansion of plasma was considered. When the spatial relaxation effects are considered, the overestimation of shock pressure in previous model is even higher than current model. The radius of plasma is assumed constant in previous model while it varies with time in current model. Obviously the shock

pressure considering plasma expansion is more realistic and more suited for micro-scale LSP.

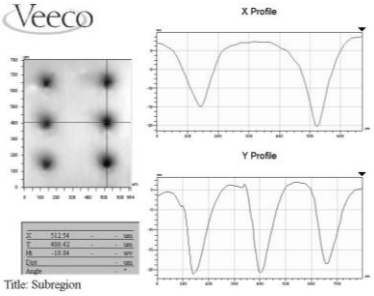

FIG. 3 MEASUREMENT OF DENT GEOMETRY USING OPTICAL PROFILOMETRY.

4.2 Deformation and Model Validation

Micro-scale LSP induced geometry deformation (dent) on copper sample is shown in Fig. 3. The dent is a clear indication of plastic deformation. SEM is used to verify that the deformation is due to shock pressure rather than thermal effects, since no thermal damage is observed around the dent. This is due to the protection of the coating layer. To quantitatively characterize the deformation, an interferometry based optical profilometer with a vertical resolution of 3 nm is used to profile the deformed regions under various conditions. Fig. 3 also shows the cross sectional measurements of dents using an optical profiler. From such profiles, the depth and the slope angle of the dents are measured and compared with simulations. The slope angle is defined as the angle between the surface normal and the average tangential line of the dent slope.

Fig. 4 (a) and (b) show the variation of dent depth and slope angle with the increase of pulse number at E = 220 μJ (3.89 GW/cm^2) for copper and nickel samples, respectively. Each experimental data point is the average of more than three features and the error bar represents standard deviation. Simulation results of current and previous shock pressure model (Zhang and Yao, 2000a) are also superposed. The current model agrees well with the experimental results while the previous model overestimates the dent depth especially at the larger number of pulses. This is primarily due to the fact that the previous model overestimated the shock pressure duration by neglecting the radial and axial expansions of the plasma (Fig. 2). When the number of pulses increases, the effect of such overestimation accumulates. This explains why the discrepancy gets larger with the number of pulses. The discrepancy in the slope angle can be similarly explained. Simulations and experiments under a wide range of other conditions showed similar trends.

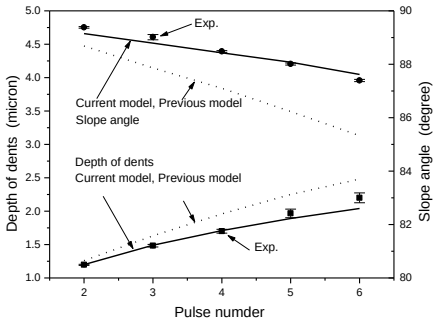

(a)

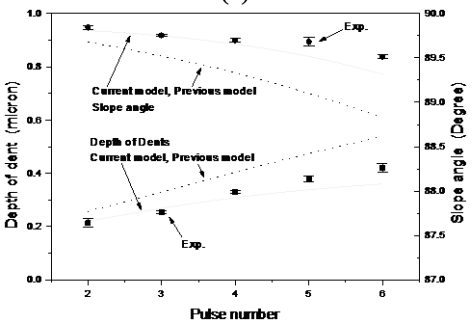

(b)

FIG. 4 DENT GEOMETRY COMPARISONS BETWEEN CURRENT MODEL AND PREVIOUS SHOCK PRESSURE MODEL, (A) COPPER, AND (B) NICKEL.

4.3 Fatigue Performance Improvement through Micro-scale LSP

Millimeter scale LSP can improve the fatigue life of metals (Clauer et al., 1981). However, it requires the use of high-energy laser pulses, which limits their pulse repetition rate to as low as 2 shocks/minute (Berthe et al., 1998). It has a limited spatial resolution and not suited for micro-scale device treatment. Micro-scale LSP has two advantages. First, it delivers laser intensities comparable to that used in the millimeter scale LSP but allows for a higher repetition rate (1kHz or higher in this paper). More importantly, the smaller footprint of treatment made possible by the smaller beam size provides greater flexibility in treating smaller devices and devices with complex geometry. Micro-scale LSP can be overlapped to treat large areas, at the same time the geometry of the laser shocked area can be controlled with micron accuracy. However the

concern is whether micro-scale LSP will improve fatigue life as millimeter scale LSP does. It is the purpose of this section to investigate this issue.

The geometry of the fatigue test specimen (Small figure in Fig. 5) is a scale down version of the standard tensile test specimen. The copper sample is 0.8 mm in thickness with two half-circle notches of radius of 0.5 mm to introduce stress concentration and more complex geometry effects. Micro scale LSP is used to treat the region between and around the notches and both sides of the specimen are shock processed. Laser pulse energy is 220 μJ. 2, 3 or 4 laser pulses at repetition rate of 1kHz are applied at each location and the shocked locations in the dotted region are spaced by 50 microns. The fatigue test was done on a material testing machine and an 80Hz sinusoidal load was applied axially. To prevent backlash, a positive mean load is applied such that the total load always oscillates in the tensile territory. It is mainly the tensile stress that is responsible for the initiation and propagation of cracks. Five pairs of tests were conducted covering the range from the fatigue strength to the ultimate strength of copper. Fig. 5 compares the typical fatigue curves of identical specimens with LSP and without LSP. It is seen that the fatigue life of the specimen with LSP is about 3 times that of the specimen without LSP.

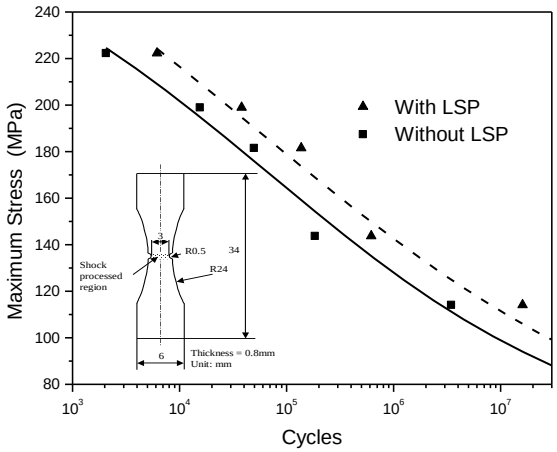

FIG. 5 RESULTS OF THE FATIGUE TEST.

Experiments shows that micro-scale LSP can increase the fatigue life of metal components as mm-scale LSP does, but its high repetition rate and high spatial resolution makes it more flexible for treating normal size samples especially those with more complex geometry. More importantly, only the micro-scale LSP offers the capability to treat micro-devices. The influence of pulse numbers on the fatigue life of copper under one of the five testing conditions (mean stress=103.5 MPa and stress oscillation amplitude=95.5MPa) had also been studied. 2, 3, and 4 pulses were applied at each location and each test was repeated three times. Contrary to intuition, the fatigue life deteriorated when more than 3 shock pulses were used although it is still much better than that without LSP. This will be explained in conjunction with the 3D simulation results.

4.4 Three-dimensional Stress/Strain Analysis

Axisymmetric stress/strain analysis was conducted for micro-scale LSP at individual locations (Zhang and Yao, 2000a & b), in which semi-infinite geometry was also assumed. Such analysis results are used in Fig. 4 of this paper to compare with experimental measurements. For LSP at overlapped locations as in the case of fatigue specimen described in the last section, 3D stress/strain analysis will be necessary. In addition, for such geometry and for small-scale specimen, the semi-infinite geometry assumption needs to be removed. Such simulation helps examine the residual stress states and understand the fatigue performance. Fig. 6 (a) shows the geometry of the fatigue sample and the distribution of *S22* on the top surface for three pulses. The simulation condition was similar to that used to process the fatigue specimen. *S22* is compressive in the shocked region including the notched area. A 2mm by 2mm region close to the notched area is shown in detail in Fig. 6(b). As seen, *S22* is compressive around the notched area and throughout the depth direction reaching a peak value of –80 MPa. Such compressive stress distribution is favorable for crack prevention and fatigue life improvement.

The distribution of *S22* is similar to that of three pulses when two pulses were used, but the compressive stress level is lower (-57MPa). When four pulses were used, *S22* becomes partially tensile in the shocked region as shown in Fig. 6(c). This counter-intuitive change is due to overly large plastic deformations in the shocked region. Large downward (33 direction) pressure primarily causes excessive deformation in the outward (11 direction) in which least resistance is experienced. Based on the constant volume principle of plastic deformation, the stress in the 22 direction becomes slightly tensile. This explains why the fatigue specimen treated with 4

pulses at each location did not perform as well as that treated with 2 and 3 pulses.

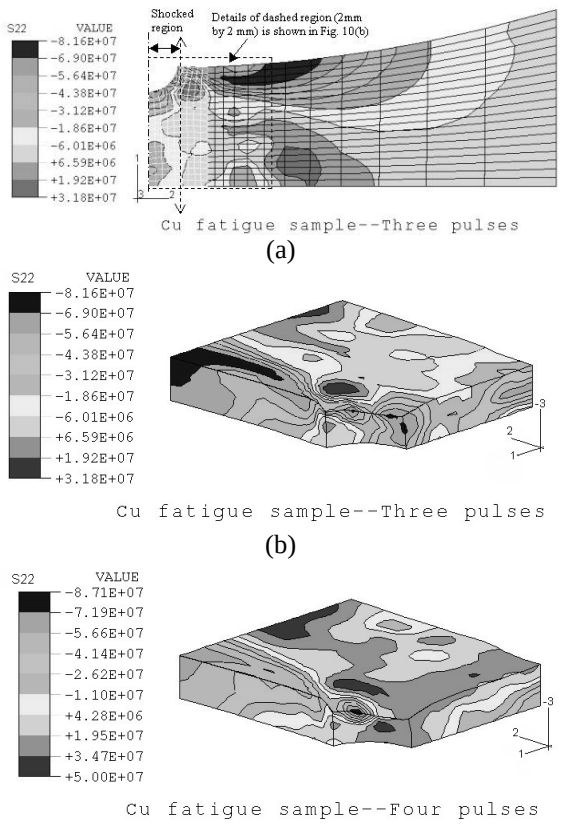

FIG. 6 RESIDUAL STRESS DISTRIBUTION OF THE LASER SHOCK PROCESSED FATIGUE SPECIMEN. (A) TOPVIEW OF THE SPECIMEN OVERLAID WITH THE *S22* DISTRIBUTION, THREE PULSES; (B) DETAILED VIEW OF THE NOTCHED REGION, THREE PULSES; AND (C) DETAILED VIEW OF THE NOTCHED REGION, FOUR PULSES. THE VOLUME SHOWN IN FIG. 6 (B) AND (C) IS 2MM IN 1-1 DIRECTION, 2 MM IN 2-2 DIRECTION, 0.2 MM IN 3-3 DIRECTION. NOTCH RADIUS IS 0.5 MM. LSP WAS CARRIED OUT AT A UNIFORM SPACING OF 50 MICRONS AND PULSE ENERGY E = 220 μJ.

4.5 Microstructure Study of Laser Shock Processed Samples

The effects of LSP on the target material can be better understood through the study of its microstructures, which are responsible for its macroscopic properties. In the past transmission electron microscopy (TEM) was used to study the dislocation density changes in high pressure (up to 100 GPa) shock processing, and dislocation cell structures in shock processed copper and nickel samples were observed (Meyers and Murr, 1981). Dislocation densities in laser shock processed and unprocessed aluminum alloys were qualitatively compared by Clauer et al. (1981) using TEM. Other aspects of microstructure changes caused by LSP, including grain orientation and texture, have not been studied. In this paper, Orientation Imaging Microscopy (OIM) was used to study the microstructure changes quantitatively. OIM has some special advantages in microstructure analysis over TEM. The sample preparation of OIM is not destructive thus the nearly original state of the sample can be observed. A much larger area than TEM can be quantitatively and statistically analyzed. The OIM micrograph accurately reproduces the features visible in the optical micrograph, but contains inherently greater crystallographic details, and the spatial resolution can reach sub-microns. OIM measurements of nickel and copper samples were carried out. A square region of the samples was shock processed (spacing of 50 microns, 2 pulses at each location, and pulse energy of 220 μJ). The samples were briefly chemical etched to remove the mechanical scratches on the surface. The shocked region was accurately located using SEM before the OIM measurements. The shocked region and shock free region were compared. A rectangular region was scanned line by line. The region was chosen to cover enough number of grains for statistic purposes. Through the indexing, the orientation of the lattice at the current location is determined. After a representative region of the sample was scanned, the statistics of the sample microstructures and lattice orientations were analyzed.

Grain Size and Uniformity, When the mean grain size is the same, the material with more uniform distribution of grain size has higher yield strength compared with the material with more scattered grain size distribution. It was found that the grain size after micro-scale LSP did not change significantly, the standard deviations of the grain size, however, for both copper and nickel were reduced by more than 20% after LSP, which means the grains become more uniform after LSP.

Subgrain Structures, Table 1 compares the microstructures of copper and nickel without and with LSP. It is observed that copper has a larger increase in substructure and in highly deformed region after LSP than nickel, while both show substantial increase in substructure and highly deformed regions with LSP compared with

that without LSP. The substructures in OIM are in fact dislocations on the top surface of the sample. The substantial increase of substructures is the major cause of strength and hardness improvement in LSP.

Table 1: Microstructure changes of copper and nickel after LSP

% of Area	Cu, no LSP	Cu, with LSP	Ni, no LSP	Ni, with LSP
With sub-structures	11±2.1	46.3±2.5	13±2.0	39.4±1.8
Highly deformed	4.4±0.9	11±1.3	0.5±0.5	4.2±0.7
Recrystallized	82.6±3.0	42.7±3.2	86.5±2.9	56.4±2.5

5. CONCLUSIONS

For micro-scale LSP, a new shock pressure model taking into account of mass, energy and momentum conservation was formulated with plasma modeled as laser supported combustion wave and its spatial expansion effects accounted for. The new model provides better correlation with experimental results in terms of deformation. Stress and strain analysis was extended to 3D and considered finite geometry, which is important for micro-scale LSP. Tests showed micro-scale LSP more than doubled the fatigue life of copper specimens under the test condition. OIM measurements quantitatively showed that LSP improved grain size uniformity. Increase of subgrain structures was also quantified and used to help explain the fatigue performance improvement by LSP. The differences between copper and nickel were explained in terms of their properties and response to shock waves.

REFERENCES

Assay, J. R., and Shahinpoor, M., (1992), *High-pressure Shock Compression of Solids*, Springer-Verlag, New York, pp. 78-82.

Berthe, L. et al., (1998), "Experimental Study of the Transmission of Breakdown Plasma Generated During Laser Shock Processing," *The European Physical Journal Applied Physics*, Vol. 3, pp 215-218.

Clauer, A. H. et al., (1981), "Effects of Laser Induced Shock Waves on Metals," *Shock Waves and High Strain Phenomena in Metals-Concepts and Applications*, Plenum, New York, pp. 675-702.

Fabbro, R. et al., (1990), "Physical Study of Laser-produced Plasma in Confined Geometry," *J. Appl. Phys.*, July, 1990, Vol. 68(2), pp. 775-784.

Murr, L. E., (1981), "Residual Microstructure--Mechanical Property Relations in Shock-Loaded Metals and Alloys," *Shock Waves and High Strain Phenomena in Metals - Concepts and Applications*, Plenum, New York, pp. 635-655.

Meyers, M. A. and Murr, L. E., (1981), *Shock Waves and High-Strain-Rate Phenomena in Metals*, Plenum Press, New York, pp. 487-530,1048.

Pirri, A. N. et al., (1978), "Plasma Energy Transfer to Metal Surfaces Irradiated by Pulsed Lasers", *AIAA Journal*, Vol. 16, No. 12, pp.1296-1304.

Peyre, P. at al., (1995), "Laser Induced Shock Waves as Surface Treatment for 7075-T7351 Aluminum Alloy," *Surf. Engng.*, Vol. 11, pp. 47-52.

Root, R. G., (1989), "Modeling of Post-Breakdown Phenomena," *Laser Induced Plasmas and Application*, Marcel Dekker, Inc., New York, pp. 95-99.

Simons, G. A., (1984), "Momentum Transfer to a Surface When Irradiated by a High-Power Laser," *AIAA Journal*, Vol. 22, No. 9, pp.1275-1280.

Vogel, A. et al., (1996), "Plasma Formation in Water by Picosecond and Nanosecond Nd:YAG Laser Pulses," *IEEE Journal of Selected Topics in Quantum Electronics*, Vol. 2, No. 4, pp. 847-871.

Zhang, W. and Yao, Y. L., (2000a), "Improvement of Laser Induced Residual Stress Distributions via Shock Waves," *ICALEO'2000, Laser Material Processing*, Vol. 89, pp. E183-192.

Zhang, W. and Yao, Y. L., (2000b), "Micro Scale Laser Shock Processing of Metallic Components," *ASME Journal of Manufacturing Science and Engineering*, accepted.

Zhang, W. and Yao, Y. L., (2001), "Modeling and Simulation Improvement in Laser Shock Processing," *ICALEO'2001,* accepted.

Zhang, H. and Yu, C., (1998), "Laser Shock Processing of 2024-T62 Aluminum Alloy," *Materials Science and Engineering A*, Vol. 257, pp. 322-327.